Frequency-Domain Analysis of Super-Regenerative Amplifiers

Jose L. Bohorquez, *Student Member, IEEE*, Anantha P. Chandrakasan, *Fellow, IEEE*, and Joel L. Dawson, *Member, IEEE*

***Abstract*—Since its invention in 1922, the super-regenerative amplifier (SRA) has been used in a variety of short-range, low-power, and/or low-cost wireless systems due to its simple implementation and excellent performance for a given power budget. Growing demand for ultralow-power receivers for short-range radios has recently reawakened an interest in the theory and design of SRAs. Building on recent work and using reasonable assumptions and approximations, we present a frequency-domain model for analyzing SRAs. We then use these models to predict the response of an SRA to arbitrary deterministic and stochastic signals including sinusoids, pulsed-sinusoids, and additive white Gaussian noise. Using the results, we present formulas for calculating the sensitivity and selectivity of SRAs. We also introduce the concept of a *trigger-time* that is particularly useful for accurately determining the optimal threshold in on-off keying (OOK) receivers and helps avoid the problems introduced by nonlinearity in SRAs. Finally, we present a prototype OOK SRA that achieves a sensitivity of −90 dBm at a bit rate of 300 kbps (BER of 10^{-3}) while consuming 500 μW, and show that its measured sensitivity matches theory within 1 dB.**

***Index Terms*—Super-regenerative amplifier (SRA), super-regenerative receiver, low power, oscillators, short-range radio.**

I. Introduction

THE super-regenerative amplifier(SRA)/receiver was first introduced by Edwin Armstrong in 1922 [1] as an exciting development in communications systems. Although it never gained the popularity of the superheterodyne receiver, recent growth in low-power, short-range wireless links has reawakened an interest in SRAs due to their excellent sensitivity for small amounts of dc power consumption [2]–[7]. The general concepts behind the operation of SRAs are intuitive, but the theory necessary for quantitative analysis tends to be mathematically tedious due to its nonlinear, time-varying nature. Thorough time-domain solutions have been available since the 1950s [8], and more recent work has focused on generalizing those results to generic SRAs [4]. Other recent work has shown the capacity to operate SRAs synchronously, improving the selectivity and data rate of SRA receivers [5], and the benefits of pulse-shaping OOK signals to optimize the sensitivity of an SRA receiver [9], [10]. Building on these works, we propose a convolution model that allows for *frequency-domain* analysis of SRAs. We then show that frequency-domain methods allow for straightforward analysis of arbitrary deterministic and stochastic input signals, and use various examples that lead to complete sensitivity equations.

As explained in [8], the SRA can be operated in four general modes combining the choices of slope-controlled versus step-controlled and linear versus logarithmic modes. The first choice describes the type of *quench signal* or *damping function* used, and the second choice describes whether the SRA output is limited to small values that prevent nonlinearities, or if its amplitude is permitted to grow to the point of compression. The subtleties of the slope- versus step-control modes will be explained in Section II, but we note that the analysis presented here is restricted to the slope-controlled mode. This method has been of greatest interest in recent literature because it offers benefits in both sensitivity and selectivity. Also, we focus our analysis mostly on the linear mode of operation. However, we introduce the concept of a *trigger-time* in Section IV-C, which is relevant to both the linear and the logarithmic modes of operation.

The paper is divided into five main sections. Section II briefly describes the general theory of the SRA and recounts the time-domain solution for its differential equation. Section III presents a convolution model of the SRA and uses it to find an SRA's response to various deterministic signals. Section IV shows how the convolution model can be used to find the SRA's response to additive white Gaussian noise (AWGN) and uses the results to calculate the expected bit error rate (BER) and sensitivity of an OOK receiver. It also introduces the concept of a trigger-time which can be used to accurately set the optimum threshold and detect signals in an OOK receiver while avoiding the problems usually caused by nonlinearity. Section V describes a test circuit used to verify the theory presented and compares measured results to those predicted using the convolution model. Section VI summarizes the key concepts and concludes the paper.

II. General SRA Theory

A. Circuit Model and Block Diagram for SRA

Fig. 1 shows the simplified (a) circuit model and (b) feedback model for an RLC-based SRA. The parameters of interest for the resonant RLC tank are: ω_0, the resonant frequency, Z_0, the characteristic impedance, Q_0, the quality factor, and ζ_0, the quiescent damping factor. The relationships between these parameters and the circuit components are

$$\omega_0 = \frac{1}{\sqrt{LC}} \tag{1}$$

$$Z_0 = \sqrt{\frac{L}{C}} = \omega_0 L = \frac{1}{\omega_0 C} \tag{2}$$

$$\zeta_0 = \frac{1}{2RC\omega_0} = \frac{1}{2Q_0} = \frac{1}{2}\frac{Z_0}{R}. \tag{3}$$

Manuscript received April 22, 2009; revised August 16, 2009. First published November 10, 2009; current version published December 09, 2009. This work was supported by the Focus Center for Circuit and System Solutions (C2S2), one of five research centers funded under the Focus Center Research Program, a Semiconductor Research Corporation program.

The authors are with the Microsystems Technology Laboratories, Massachusetts Institute of Technology, Cambridge, MA 02139 USA (e-mail: joselb@mit.edu; anantha@mtl.mit.edu; jldawson@mtl.mit.edu).

Digital Object Identifier 10.1109/TMTT.2009.2033843

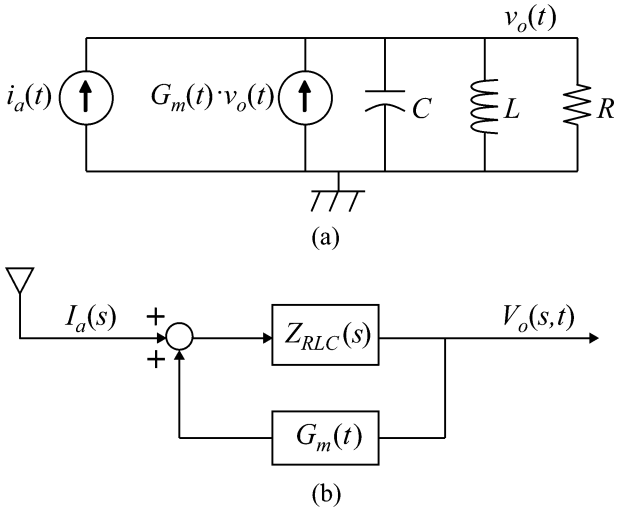

Fig. 1. (a) SRA circuit model and (b) SRA feedback loop model.

Using these parameters, the impedance for a parallel resonant tank can be written as

$$Z_{\mathrm{RLC}}(s) = \frac{Z_0\omega_0 s}{s^2 + 2\zeta_0\omega_0 s + \omega_0^2}. \tag{4}$$

If $G_m(t)$ varies slowly enough with respect to ω_0, such that the system in Fig. 1 is quasi-static, we can define a time-varying transfer function for the feedback loop shown in Fig. 1(b) by

$$Z_{TV}(s,t) = \frac{V_o(s,t)}{I_a(s)} = \frac{Z_{\mathrm{RLC}}(s)}{1 - G_m(t)\cdot Z_{\mathrm{RLC}}(s)} \tag{5}$$

which can be rewritten as

$$Z_{TV}(s,t) = \frac{Z_0\omega_0 s}{s^2 + 2\zeta(t)\omega_0 s + \omega_0^2} \tag{6}$$

where $\zeta(t)$ is the *instantaneous damping factor* or *damping function* and is defined as

$$\zeta(t) = \zeta_0(1 - G_m(t)R). \tag{7}$$

Note that (6) only differs from (4) in the denominator where ζ_0 is replaced by $\zeta(t)$. This is because the positive feedback from transconductance $G_m(t)$ can be modeled as a negative resistance that only affects the damping factor of the second-order system in Fig. 1.

B. SRAs as Time-Varying, Second-Order Systems

An SRA differs from a linear time-invariant (LTI) system in that its poles are periodically shifted between the left-hand side and right-hand side of the complex plane by varying the damping function $\zeta(t)$. The exact function used to define $\zeta(t)$ determines the characteristics of the SRA's response to an input signal, and various functions can and have been used [3], [7]. As an example, Fig. 2 shows the instantaneous value of the poles of an SRA as $\zeta(t)$ is linearly varied during one cycle using a ramp function. As will be shown, for each period, the resulting time-varying system yields a filtered and amplified sample of its input signal's envelope. Unlike LTI systems whose filtering qualities are strictly dependent on the static location of their poles and zeros, the filtering qualities of SRAs additionally depend on the characteristics of the damping function used to vary their pole locations. Furthermore, in contrast with LTI systems, SRAs exploit the instability portion of their cycle to achieve very high gain despite using active components that provide relatively small gain.

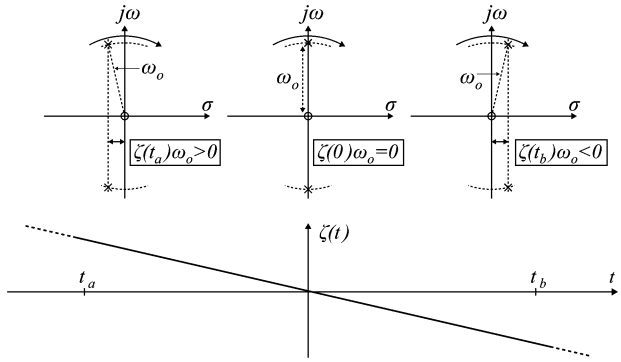

Fig. 2. Time-varying pole/zero locations for an SRA as the damping function changes.

C. General SRA Solution for Linear Mode Operation

Historically, SRAs have been used in either the *linear* or *logarithmic* mode [4], [8]. In the linear mode, the SRA is configured such that its *output* remains small enough throughout each quench cycle to prevent significant nonlinearities. As a result, the envelope of the SRA's output is proportional to the amplitude of the input signal. In the logarithmic mode, the SRA is configured such that its output saturates during each cycle. The integral of its envelope is then proportional to the logarithm of the input signal's amplitude. The following analysis is valid for the linear mode, but later discussions will show how the results can be used to accurately model an SRA that is allowed to enter compression.

Using (6) we can write the following differential equation to describe the LTV model of the SRA in Fig. 1:

$$v_o''(t) + 2\zeta(t)\omega_0 v_o'(t) + \omega_0^2 v_o(t) = 2R\zeta_0\omega_0 i_a'(t). \tag{8}$$

A more general version of (8) and its thorough solution can be found in [4], where the general solution is broken down into the sum of the free response and the forced response. The following analysis assumes that the free response is zero. In a practical implementation, this means that any oscillation from a previous cycle is *quenched* before time t_a when a new cycle begins. This simplifies the mathematics, but more importantly, it improves the performance of the receiver since it ensures that each cycle is independent of all previous cycles. Mathematically, the quenching is done by allowing the poles to remain in the left-hand side long enough for the envelope of the output voltage to decay below the noise levels. To expedite the decay, the poles can be pushed far to the left, or equivalently, the damping function can be made a large positive value. Practically, this can be done by briefly shorting the tank as in [11] or by reducing the transconductance, $G_m(t)$, to a very low value as in [2].

The general solution found in [4] can be modified for the specific case of an RLC-based SRA with an input current $i_a(t)$,

resulting in the output voltage

$$v_o(t) = Z_0 e^{-\omega_0 \int_0^t \zeta(\lambda)d\lambda} \times \int_{t_a}^{t} i_a'(\tau) e^{\omega_0 \int_0^\tau \zeta(\lambda)d\lambda} \sin[\omega_0(t-\tau)]d\tau. \quad (9)$$

In (9), $\zeta(t)$ is defined such that it is positive for $t_a \leq t < 0$ and negative for $0 \leq t \leq t_b$ as in Fig. 2. The solution can be broken down into the time-dependent gain $\mu(t)$ and the filtering term $k(t)$

$$v_o(t) = Z_0 \mu(t) k(t) \quad (10)$$

where

$$\mu(t) = e^{-\omega_0 \int_0^t \zeta(\lambda)d\lambda} \quad (11)$$

$$k(t) = \int_{t_a}^{t} i_a'(\tau) g(\tau) \sin[\omega_0(t-\tau)]d\tau \quad (12)$$

$$g(t) = e^{\omega_0 \int_0^t \zeta(\lambda)d\lambda}. \quad (13)$$

The gain component $\mu(t)$ reaches its peak at $t = t_b$ and its maximum value $\mu(t_b)$ is referred to as the super-regenerative gain [8]. The term $g(t)$ is referred to as the sensitivity function and has a peak value of unity at $t = 0$. For common damping functions it decays rapidly outside of a time window concentrated about $t = 0$, limiting the effect of the input signal $i_a(t)$ outside of that window. This quality will be exploited in Section III to approximate $k(t)$ by a convolution and perform frequency-domain analysis of the SRA. For *slope-controlled* SRAs, $\zeta(t)$ changes slowly enough that multiple periods of the input signal occur during the sensitivity period [8]. If $\zeta(t)$ changes from positive to negative abruptly, the SRA is said to be operating in the *step-controlled* region and has a significantly different frequency response. The subsequent analysis assumes the SRA is operated in the slope-controlled mode, which is preferable as it achieves better sensitivity and selectivity [8].

D. SRA Solution for a Ramp and Sine Damping Functions

Almost any arbitrary shape can be used as the damping function $\zeta(t)$ as long as it is positive for $t_a \leq t < 0$ and negative for $0 < t \leq t_b$. Two common waveforms in slope-controlled SRAs are the ramp (or sawtooth) and the sine-wave [3]–[5], [7], [9], [11]. The ramp damping function proves particularly useful for analysis since it leads to Gaussian equations that have closed-form solutions. Furthermore, it achieves higher gain and has a frequency response preferable to that of sine-wave damping as discussed in this section and Section III-B.

For the time span $t_a \leq t < t_b$, the ramp damping function has the form

$$\zeta(t) = -\beta t \quad (14)$$

where β is its slope and has units of s^{-1}. Substituting (14) into (11) and (13) results in

$$\mu_{\mathrm{ramp}}(t) = e^{\frac{1}{2}\omega_0 \beta t^2} = e^{\frac{t^2}{2\sigma_s^2}} \quad (15)$$

$$g_{\mathrm{ramp}}(t) = e^{-\frac{1}{2}\omega_0 \beta t^2} = e^{-\frac{t^2}{2\sigma_s^2}} \quad (16)$$

where

$$\sigma_s = \frac{1}{\sqrt{\omega_0 \beta}} \quad (17)$$

has units of $\mathrm{s}/\sqrt{\mathrm{rad}}$ and is defined as the *SRA time constant*.

The sine-wave damping function has the form

$$\zeta(t) = -\frac{\beta}{\omega_q} \sin(\omega_q t) \quad (18)$$

where

$$\omega_q = \frac{2\pi}{t_b - t_a}. \quad (19)$$

It is defined such that its slope is $-\beta$ at $t = 0$. Substituting (18) into (11) and (13) results in

$$\mu_{\sin}(t) = \exp\left(\frac{1 - \cos(\omega_q t)}{\omega_q^2 \sigma_s^2}\right) \quad (20)$$

$$g_{\sin}(t) = \exp\left(-\frac{1 - \cos(\omega_q t)}{\omega_q^2 \sigma_s^2}\right). \quad (21)$$

To facilitate the comparison between these two damping functions, we set $t_b = |t_a| = T_q/2$, where T_q is the quench period, and define the ratio

$$\gamma = \frac{t_b}{\sigma_s} = \frac{T_q}{2\sigma_s}. \quad (22)$$

This allows us to make the substitution $\omega_q = \pi/(\gamma\sigma_s)$. Using (22) and solving (15) and (20) at $t = t_b$ allows us to evaluate the super-regenerative gain for both damping functions as

$$\mu_{\mathrm{ramp}}(t_b) = e^{\frac{1}{2}\gamma^2} \quad (23)$$

$$\mu_{\sin}(t_b) = e^{\frac{2}{\pi^2}\gamma^2}. \quad (24)$$

The ratio between the two gains is

$$\frac{\mu_{\mathrm{ramp}}(t_b)}{\mu_{\sin}(t_b)} = e^{(\frac{1}{2} - \frac{2}{\pi^2})\gamma^2} \approx e^{0.3\gamma^2}. \quad (25)$$

For a ratio of $\gamma = 3$, the gain of the SRA using a ramp damping function is $14.5\times$ greater (23 dB) compared with the sine-wave damping function. Of course the amplitude of the sine-wave damping function could be increased to increase its gain, but this would widen the bandwidth of the SRA, increasing noise and degrading selectivity. This will be shown in Section III-B along with the effects of γ on the frequency response of the SRA. Fig. 3 shows $g_{\mathrm{ramp}}(t)$ and $g_{\sin}(t)$ for $\gamma = 3$. For time values near zero, the two sensitivity functions are similar. However, g_{ramp} approaches zero more quickly and is reduced to 0.01 at $t_b = 3\sigma_s$ while $g_{\sin}$ is only reduced to 0.161. Later sections show this gives the ramp damping function a superior frequency response. Generally speaking, the SRA's gain grows exponentially with γ and the frequency response improves. For a given value of σ_s, this requires longer quench cycles and, therefore, lower bit rates creating a tradeoff. The tradeoff favors increasing γ, however, since the gain grows as e^{γ^2} whereas the bit rate is reduced linearly.

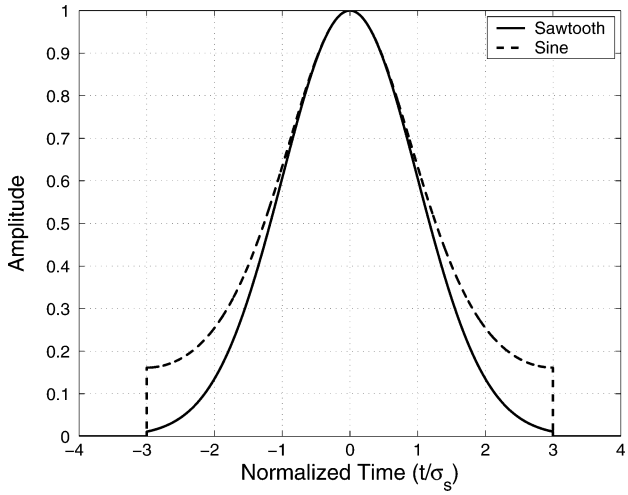

Fig. 3. Sensitivity functions for sawtooth/ramp and sine damping functions ($\gamma = 3$).

III. Convolution Model of SRA Solution

In this section, we show that (12) closely resembles a convolution and exploit this quality to perform frequency-domain analysis on the SRA. Typically, we are interested in the value of the envelope of $v_o(t)$ near the end of the cycle ($t \approx t_b$), since that is when the maximum super-regenerative gain is achieved. Since the output is oscillatory, we are not interested in its value exactly at t_b, but rather at some time near t_b when the sinusoidal term is at its peak. In that time range, (12) can be rewritten as the nearly exact approximation

$$k(t) \approx \int_{-\infty}^{\infty} x(\tau)\Pi\left(\frac{\tau}{t_b - t_a}\right)\sin(\omega_0[t-\tau])d\tau \qquad (26)$$

where

$$x(t) = i_a'(t)g(t). \qquad (27)$$

$$\Pi(x) = \begin{cases} 1 & \text{if } |x| < 1/2 \\ 0 & \text{otherwise.} \end{cases} \qquad (28)$$

The approximation in (26) assumes $t_b \approx -t_a$, although this assumption is not necessary and can be avoided at the expense of increased complexity by modifying the argument of $\Pi(t)$. Equation (26) can be rewritten as the convolution

$$k_*(t) = x(t)\Pi\left(\frac{t}{t_b - t_a}\right) * \sin(\omega_0 t) \qquad (29)$$

which is valid for time $t \approx t_b$. Note that if the value of $k(t)$ is desired near some time other than t_b, that time instant can be substituted in the argument of $\Pi(t)$.

As discussed in Section II-D, $g(t)$ always has a maximum value of unity at $t = 0$, and typically drops sharply for $|t| > 3\sigma_s$. Fig. 4 illustrates the effects of this property on (12) when $i_a(t)$ is the sinusoid

$$i_a(t) = I_a \sin(\omega_a t + \phi_a). \qquad (30)$$

As shown in Fig. 4(a) and(b), $g(t)$ grows to a maximum value of unity as the damping function approaches zero. Fig. 4(c) illustrates the time derivative of $i_a(t)$, and Fig. 4(d) shows $x(t)$ which has the form of a time-windowed version $i_a'(t)$. As shown

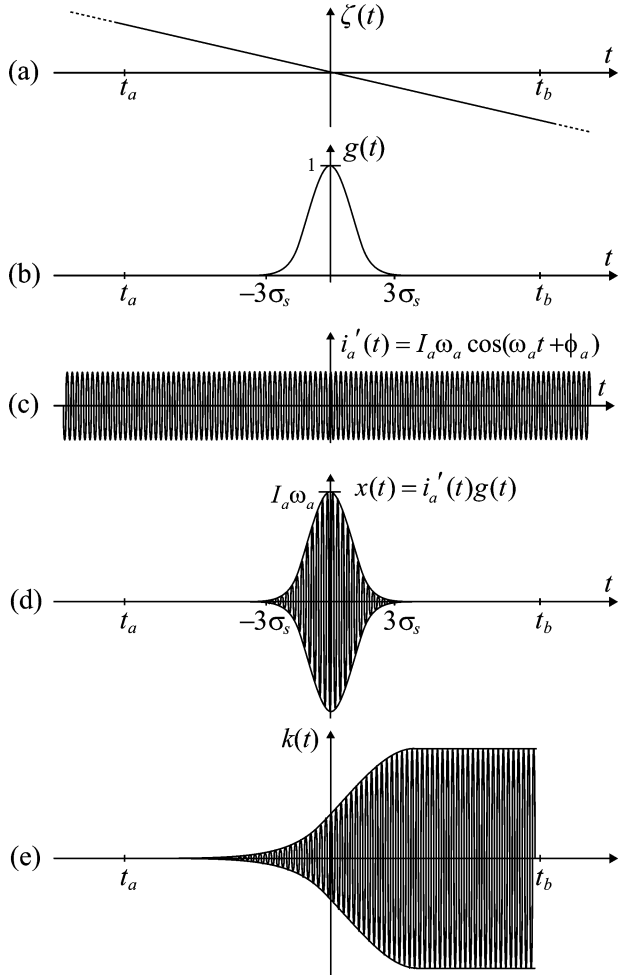

Fig. 4. (a) Damping function, (b) sensitivity function, (c) time derivative of sinusoidal input, (d) windowed input, and (e) $k(t)$.

in Fig. 4(e), $k(t)$ is oscillatory and grows for $t < 3\sigma_s$, but then flattens out. This occurs because $x(t)$ becomes very small for values of $t > 3\sigma_s$. As mentioned previously, $k_*(t)$ is only valid (and nearly exact) for $t \approx t_b$. However, Fig. 5 shows that it is generally a very good approximation for values of $t \geq 3\sigma_s$. In fact, if $\gamma \geq 3$, (29) can be simplified further by removing the $\Pi(t)$ term without much loss to accuracy since $x(t)$ is very nearly zero for $|t| > 3\sigma_s$

$$k_*(t) \approx x(t) * \sin(\omega_0 t). \qquad (31)$$

This approximation has the same effect as setting $\gamma = \infty$ (for $k(t)$, but not $\mu(t)$) and results in an optimistic estimate of the frequency response. Nonetheless, we will use this approximation for the subsequent hand calculations and then show numerical examples that clarify its effects.

A. SRA Response to an Arbitrary Input

The key benefit to the convolution model is that it enables the use of frequency-domain techniques that facilitate the analysis of an SRA's response to arbitrary input signals. Taking the Fourier transform of (31) yields the frequency-domain signal

$$K_*(\omega) = j\pi(X(\omega_0)\delta(\omega - \omega_0) - X(-\omega_0)\delta(\omega + \omega_0)). \qquad (32)$$

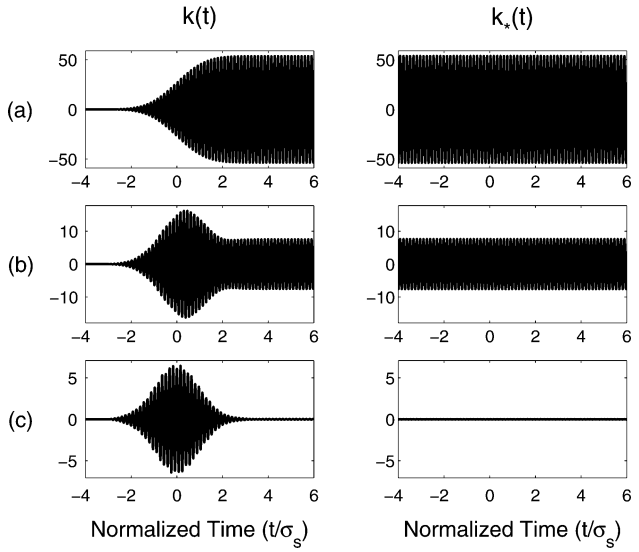

Fig. 5. Numerical simulations comparing the exact equation $k(t)$ with the convolution approximation $k_*(t)$ for $\gamma = 3$ and (a) $\omega_a = \omega_0$, (b) $\omega_a = \omega_0 + 2\Omega_s$, and (c) $\omega_a = \omega_0 + 4\Omega_s$.

The time convolution of $x(t)$ with a sinusoid yields the result that only the values of $X(\omega)$ at $\omega = \pm\omega_0$ are important. Taking the inverse Fourier transform of (32) gives $k(t)$ for an arbitrary input signal $i_a(t)$

$$k_*(t) = |X(\omega_0)| \sin\left(\omega_0 t + \angle X(\omega_0)\right). \tag{33}$$

Since $x(t)$ is the time-domain product of $i_a'(t)$ and $g(t)$, its Fourier transform is the convolution

$$X(\omega) = \frac{1}{2\pi} j\omega I_a(\omega) * G(\omega). \tag{34}$$

Substituting (33) into (10) yields the solution for the output voltage of the SRA which is usually accurate for $t > 3\sigma_s$

$$\boxed{v_o(t) = Z_0 \mu(t) |X(\omega_0)| \sin\left(\omega_0 t + \angle X(\omega_0)\right).} \tag{35}$$

A more accurate solution can be used for numerical analysis that incorporates the $\Pi(t)$ term in (29) by using the function

$$X_\Pi(\omega) = X(\omega) * (t_b - t_a) \mathrm{sinc}\left(\frac{1}{2\omega(t_b - t_a)}\right) \tag{36}$$

in place of $X(\omega)$ in (34).

Equations (35) and (34) define the general form of an SRA's output. For an input current $i_a(t)$, the output voltage is proportional to the resonator's characteristic impedance Z_0, its envelope grows exponentially, its filtering characteristics are determined by the sensitivity function $g(t)$, and it oscillates at its resonant frequency.[1] Typically, SRAs are used in amplitude modulation systems where the phase of the input signal carries no information. As a result, the sinusoidal term in (35) is often removed by connecting the output of the SRA to an envelope detector whose output is

$$v_e(t) = Z_0 \mu(t) |X(\omega_0)|. \tag{37}$$

B. SRA Response to a Sinusoidal Input

The filtering qualities of the SRA become more clear by analyzing its response to a sinusoidal input. For the input signal (30), (34) becomes

$$X(\omega) = \frac{\omega_a I_a}{2} \left(G(\omega + \omega_a) e^{-j\phi_a} + G(\omega - \omega_a) e^{j\phi_a}\right). \tag{38}$$

It is illustrative to use a specific example of a sensitivity function to appreciate the qualities of $G(\omega)$. For the ramp damping function described in Section II-D, $g(t)$ is Gaussian, such that its Fourier transform is also Gaussian

$$G(\omega) = \frac{\sqrt{2\pi}}{\Omega_s} e^{-\frac{\omega^2}{2\,\Omega_s^2}} \tag{39}$$

where

$$\Omega_s = \frac{1}{\sigma_s} = \sqrt{\omega_0 \beta} \tag{40}$$

is the *SRA frequency constant*. As a result, when $X(\omega)$ is evaluated at ω_0, the term $G(\omega_0 + \omega_a)$ is practically zero and (38), evaluated at ω_0, simplifies to

$$X(\omega_0) = \frac{\omega_a I_a}{2} G(\omega_0 - \omega_a) e^{j\phi_a}. \tag{41}$$

Substituting (41) into (35) yields the SRA's output for a sinusoidal input

$$\boxed{v_o(t) = \tfrac{Z_0 \omega_a I_a}{2} \mu(t) |G(\omega_0 - \omega_a)| \sin(\omega_0 t + \phi_a).} \tag{42}$$

For the specific case of the ramp damping function (14), the SRA's output is

$$v_o(t) = \frac{I_a Z_0}{2} \frac{\omega_a \sqrt{2\pi}}{\Omega_s} \cdot e^{\frac{-(\omega_0 - \omega_a)^2}{2\,\Omega_s^2}} \cdot e^{\frac{t^2}{2\sigma_s^2}} \sin(\omega_0 t + \phi_a). \tag{43}$$

Fig. 6 shows a graphical representation of the mathematics used to find (42) and (43). Since the input signal is sinusoidal, its time derivative, $i_a'(t)$, effectively "up-converts" $g(t)$ and translates its spectrum to $\pm\omega_a$. The resulting bandpass signal $x(t)$ is then convolved with $\sin(\omega_0 t)$ which is equivalent to multiplying its spectrum $X(\omega)$ with two Dirac delta functions. The result is a sinusoidal term $k_*(t)$ whose amplitude depends on the magnitude of $X(\omega)$ evaluated at $\omega = \pm\omega_0$. Finally, the sinusoidal term $k_*(t)$ is multiplied by the SRA's time-dependent gain resulting in $v_o(t)$.

Solution (42) is valid for general damping functions while (43) describes the response of an SRA with a ramp damping function. There are five important observations that can be made from (43) that are generally true for other damping functions. First, the output voltage is linearly proportional to the amplitude of the input current and the characteristic impedance of the

[1]Since this is the result of linear analysis, the injection locking phenomenon is not modeled. For a large input signal whose frequency is close to ω_0, the oscillation frequency may become the same as the input signal's as the output of the SRA grows and nonlinearities take effect. However, since it is the envelope of the output that is of interest, this does not affect the practical operation of the SRA.

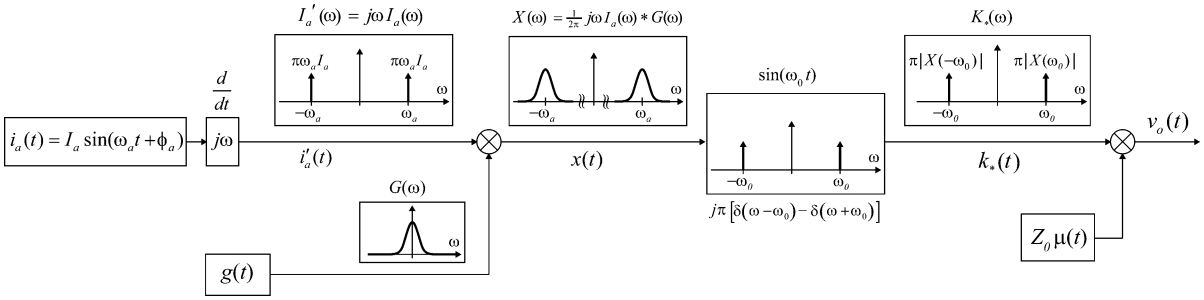

Fig. 6. Graphical representation of SRA response to a sinusoidal input signal.

resonant tank. Second, there is a constant gain term that depends on the damping function and the input signal's frequency. Third, the SRA filters the input current with a Gaussian-shaped filter centered about the tank's resonant frequency, ω_0, with a bandwidth defined by the frequency constant, Ω_s. Fourth, the output voltage has an envelope that grows very rapidly (an exponential with a squared time exponent) and is dependent on σ_s. And fifth, the output voltage is oscillatory with a frequency equal to the tank's resonant frequency.

The constant Ω_s and its inverse, σ_s, practically define the response of the system in terms of both frequency selectivity and gain. Since ω_0 is set by the application requirements, (43) shows that the only two design variables are β, the slope of the damping function, and Z_0. If the slope of the damping function is reduced, selectivity improves but gain is reduced. To achieve the same gain, each cycle must be longer (since the gain increases with time) resulting in a bit rate reduction. However, the tradeoff between gain, bandwidth, and bit rate are not linear as with most systems since the bit rate and bandwidth are inversely proportional to σ_s, whereas gain grows as e^{t^2/σ_s^2}. This means that bit rate and bandwidth are traded for the square root of the log of gain.

Fig. 7 illustrates the frequency response of the SRA for various values of γ. The $\gamma = \infty$ waveform represents the result of the approximation used in (31) where the limits of integration are extended to $\pm\infty$. The other lines show that the primary effect of reducing γ is a degradation in the frequency response of the SRA manifested by rising sidelobes. However, for $\gamma \geq 3$ the SRA provides more than 55 dB of attenuation in the stopband, confirming that (31) is a good approximation. Fig. 8 compares the frequency response of the ramp and sine-wave damping functions discussed in Section II-D and confirms that the ramp damping function is preferable since it achieves higher gain and lower sidebands for a given value of γ.

The fact that a system with a single active device with very small intrinsic gain is able to filter and amplify with almost limitless gain speaks to the SRA's compelling potential in low-power applications. The analysis above also shows a peculiar quality of the super-regenerative receiver: its filter bandwidth is not strictly a function of resistance, capacitance, and inductance, but also of the characteristics of its damping function. This means that high selectivity can be achieved despite limitations in the Q of an LC resonator.

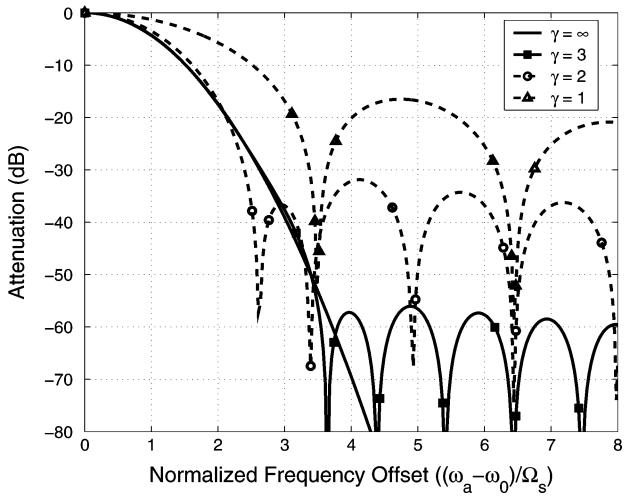

Fig. 7. Frequency response using a sawtooth/ramp damping function and varying values of γ.

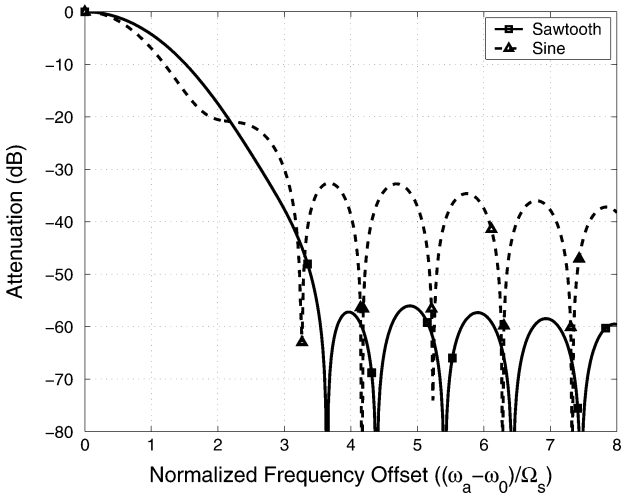

Fig. 8. Frequency response using a sawtooth/ramp and sine damping functions ($\gamma = 3$).

C. SRA Response to Multiple Sinusoids

Analyzing the SRA's response to multiple sinusoidal inputs is simplified by the convolution model since superposition holds. For an input signal comprising the sum of multiple sinusoidal inputs

$$i_a(t) = \sum_n I_n \sin(\omega_n t) \tag{44}$$

$|X(\omega_0)|$ is evaluated using (34) and superposition

$$|X(\omega_0)| = \sum_n \frac{1}{2}\omega_n I_n |G(\omega_0 - \omega_n)|. \tag{45}$$

The $|G(\omega_0+\omega_n)|$ terms are ignored because $G(\omega)$ is a baseband signal. This result can be combined with subsequent results to analyze the effect of blockers on the performance of the SRA.

D. SRA Response to a Pulse-Shaped Sinusoidal Input

Recent publications show that there is a benefit to using spread-spectrum techniques in super-regenerative receivers to improve their sensitivity [9], [12]. This can be done by shaping OOK pulses, such that a *one* is represented by the pulsed sinusoid

$$i_a(t) = \frac{T_q}{E_p} p(t) I_a \sin(\omega_0 t) \tag{46}$$

where T_q is the quench period and

$$E_p = \int_{-\infty}^{\infty} p^2(t)dt = \frac{1}{2\pi}\int_{-\infty}^{\infty} |P(\omega)|^2 d\omega \tag{47}$$

is the energy of the normalized pulse. The pulse $p(t)$ is defined to have a maximum value of unity at $t = 0$ and is equal to zero for $t < t_a$ and $t > t_b$. The term T_q/E_p is used such that the pulse-shaped input signal has the same energy over a quench period as a CW input signal. The input signal (46), has the spectrum

$$I_a(\omega) = \frac{jI_aT_q}{2E_p}(P(\omega+\omega_0) - P(\omega-\omega_0)). \tag{48}$$

Substituting (48) in (34) and evaluating $|X(\omega)|$ at ω_0 yields

$$|X(\omega_0)| = \frac{I_aT_q}{4\pi E_p}\left|\int_{-\infty}^{\infty}(\omega_0-\lambda)P(2\omega_0-\lambda)G(\lambda)d\lambda + \int_{-\infty}^{\infty}(\omega_0-\lambda)P(-\lambda)G(\lambda)d\lambda\right|. \tag{49}$$

Since both $P(\omega)$ and $G(\omega)$ are baseband signals, the first integral in (49) can be discarded, yielding

$$|X(\omega_0)| = \frac{I_aT_q}{4\pi E_p}\left|\int_{-\infty}^{\infty}\omega_0 G(\lambda)P(-\lambda)d\lambda - \int_{-\infty}^{\infty}\lambda G(\lambda)P(-\lambda)d\lambda\right|. \tag{50}$$

If $g(t)$ and $p(t)$ are even-symmetric, which is usually the case, their Fourier transforms are real and even-symmetric, making the second integral zero. Even without symmetry, this term is negligible since $\lambda \ll \omega_0$ for values of $G(\lambda)P(-\lambda)$ that are significant. This means that the second integral in (50) can be discarded, leaving

$$|X(\omega_0)| = \frac{\omega_0 I_aT_q}{4\pi E_p}\left|\int_{-\infty}^{\infty} G(\lambda)P(-\lambda)d\lambda\right|. \tag{51}$$

This can be interpreted to mean that $|X(\omega_0)|$ is proportional to the cross-correlation of $G(\omega)$ and $P(-\omega)$.

Solving this convolution and substituting its result in (42) gives the response of the SRA to a general pulse-shaped sinusoidal input. Time-domain techniques are used in [9] to show that there is an optimum pulse shape that results in the maximum output signal energy for a given input signal energy. This can also be shown in the frequency domain by finding the pulse shape that maximizes $|X(\omega_0)|$. By Schwarz's inequality

$$|X(\omega_0)|^2 = \left(\frac{\omega_0 I_aT_q}{4\pi E_p}\right)^2\left|\int_{-\infty}^{\infty}P(-\lambda)G(\lambda)d\lambda\right|^2 \le \left(\frac{\omega_0 I_aT_q}{2E_p}\right)^2 E_pE_g \tag{52}$$

with equality occurring only if $P(-\omega) = G(\omega)$, a condition achieved if $p(t) = g(t)$.[2] In that case, $|X(\omega_0)|$ is

$$|X(\omega_0)| = \frac{1}{2}\omega_0 I_aT_q. \tag{53}$$

This means that, for a given input signal energy, the output signal energy is maximized if $p(t) = g(t)$. In that case, the output signal energy is independent of the damping function and input pulse shape or energy. Instead it depends on the signal's amplitude, the SRA's resonant frequency, and the quench frequency. Note that using the optimal pulse shape comes at the expense of a wider transmitted signal. This is not always beneficial if a narrow transmission spectral mask is required. However, for spread spectrum (e.g., ultrawide band) systems, this could be exploited to maximize the sensitivity of a super-regenerative receiver [9], [10].

IV. Receiver Sensitivity Analysis

Modern SRA-based digital receivers are used almost exclusively to demodulate OOK signals. Their task is to detect whether a given transmitted bit was a *one* or a *zero*. For linear-mode SRA's, the actual detector implementation usually involves using a filter or envelope detector to measure the peak amplitude of the SRA's output, which occurs at time t_b. Since the phase information of the incoming signal is lost, the receiver is inherently non-coherent. When a *one* is sent, the signal at the input of the SRA is a pulsed sinusoid, and when a *zero* is sent, the input signal is modeled as additive white Gaussian noise (AWGN) (ignoring blockers). To calculate the sensitivity of the receiver, the probability density functions of these two cases must be solved. Any gain component that is common to both, such as $\mu(t_b)$, can be ignored since it does not affect the signal-to-noise ratio of the output signal. As a result, only the statistics of $|X(\omega_0)|$ in (35) [or (37)] are needed. It is important to note that $|X(\omega_0)|$ is not a function of time and can, therefore, be treated as a constant. To simplify the notation and clarify that it is a current, we define

$$I_X = |X(\omega_0)|. \tag{54}$$

Since the input signal contains a stochastic component, $\mathbf{I_X}$ is a random variable.[3] To find the BER of the system for a given input signal amplitude, we must find the probability density

[2]Schwarz's inequality allows for an arbitrary constant of proportionality that is omitted here since $p(t)$ and $g(t)$ have normalized peak values of unity by definition.

[3]Bold typeface is used to denote a random variable.

functions for $\mathbf{I_X}$ given that a *one* or a *zero* was transmitted; respectively $p_{\mathbf{I_X}}(i_X \mid s_m = 1)$ and $p_{\mathbf{I_X}}(i_X \mid s_m = 0)$.

When a *zero* is transmitted, the incoming signal is strictly AWGN. Since $\mathbf{X}(\omega)$ is the result of linear operations on Gaussian noise, it too has a Gaussian density function (though it is no longer white). $\mathbf{X}(\omega_0)$ is, therefore, a Gaussian random variable, and $\mathbf{I_X}$, being its absolute value, has the Rayleigh density

$$p_{\mathbf{I_X}}(i_X \mid s_m = 0) = \frac{i_X}{\sigma_X^2} e^{-i_X^2/2\sigma_X^2} \tag{55}$$

where σ_X^2 is the variance of $\mathbf{I_X}$ [13].

When a *one* is transmitted, the incoming signal can be modeled as the sum of a pulse-shaped sinusoid and AWGN, resulting in a rician density. However, for acceptable BER, the signal power must be considerably larger than the noise power, allowing a Gaussian density approximation for $\mathbf{I_X}$

$$p_{\mathbf{I_X}}(i_X \mid s_m = 1) = \frac{1}{\sigma_X \sqrt{2\pi}} e^{-(i_X - I_s)^2/2\sigma_X^2} \tag{56}$$

where I_s is the value of $|X(\omega_0)|$ in response to a pulsed sinusoidal input signal of amplitude I_a and frequency ω_0. For a general pulse shape and damping function, I_s can be calculated using (51) as

$$I_s = \frac{1}{2}\omega_0 I_a K_c \tag{57}$$

where

$$K_c = \frac{1}{2\pi}\left|\int_{-\infty}^{\infty} G(\lambda)P(-\lambda)d\lambda\right| \tag{58}$$

is defined as the *correlation coefficient* [13]. However, there are two specific cases of particular interest.

1) *Case 1*, $p(t) = 1$: For the case with no pulse shaping, I_s can be derived using (41)

$$I_{s1} = \frac{1}{2} I_a \omega_0 G(0). \tag{59}$$

For the specific case of a ramp damping function, I_s is

$$I_{s1} = \frac{1}{2} I_a \omega_0 \sigma_s \sqrt{2\pi}. \tag{60}$$

2) *Case 2*, $p(t) = g(t)$: When the pulse shape is matched to the sensitivity function, I_s is the same as (53)

$$I_{sg} = \frac{1}{2} I_a \omega_0 T_q. \tag{61}$$

From the analysis presented in Section III-D, the signal energy should be maximized for $p(t) = g(t)$. For any sensitivity function, the benefit achieved by using that optimized pulse signal, therefore, is

$$\frac{I_{sg}}{I_{s1}} = \frac{T_q}{G(0)}. \tag{62}$$

Since the output noise power is the same in both cases, this gives a direct measure of the benefit in output signal-to-noise ratio. For the specific case of a ramp damping function, the benefit is

$$\frac{I_{sg}}{I_{s1}} = \frac{T_q}{\sigma_s \sqrt{2\pi}} = \frac{2\gamma}{\sqrt{2\pi}} \tag{63}$$

making the substitution defined in (22). Recall, however, that (59) is based on the approximation in (53) which improves in accuracy for larger values of γ and becomes very accurate for $\gamma \geq 3$. For a value of $\gamma = 3$, the improvement in sensitivity is 7.6 dB. It bares repeating that this benefit comes at the expense of a wider transmitted signal.

The final step required to find the sensitivity of an SRA is to solve for σ_X^2, the variance of $\mathbf{I_X}$.

A. Noise Analysis Using the Convolution Model

The convolution model is particularly useful for analyzing an SRA's response to noise. The noise component of the input signal is modeled as a current $i_n(t)$ with the power spectral density (PSD)

$$S_n(\omega) = \frac{N}{2}. \tag{64}$$

It is important to recall that noise and sinusoids are power signals with PSDs (i.e., they have infinite energy, but finite power). The sensitivity function $g(t)$, however, is an energy signal and does not have a PSD; instead it has an energy spectral density (ESD) [13]. Multiplying a power signal with an energy signal results in an energy signal, so $x(t)$ is an energy signal and its ESD is the frequency-domain convolution of $S_n'(\omega)$ and $|G(\omega)|^2$:

$$\overline{|X(\omega)|^2} = \frac{\omega^2}{2\pi} S_n(\omega) * |G(\omega)|^2 = \frac{N\omega^2}{4\pi} * |G(\omega)|^2. \tag{65}$$

The overline in (65) is used to signify *expected value* since $x(t)$ is a random process and its Fourier transform, $X(\omega)$, is also random. Appendix A shows that this convolution, evaluated at ω_0 simplifies to

$$\sigma_X^2 = \overline{|X(\omega_0)|^2} = \frac{1}{2} N \omega_0^2 E_g. \tag{66}$$

For the specific case of a ramp damping function, $E_g = \sigma_s\sqrt{\pi}$.

The variance σ_X^2 is a measure of the output noise energy, whereas I_s^2 is a measure of the output signal energy. The sensitivity of the receiver can be solved using these two quantities and the density functions (55) and (56).

B. Solving for the BER and Sensitivity

As shown in [13], the error probability for an OOK receiver with densities (55) and (56) can be closely approximated as

$$P_e = \frac{1}{2} e^{-\frac{I_s^2}{8\sigma_X^2}}. \tag{67}$$

Assuming that *ones* and *zeros* are equally likely means that the power received is

$$P_{Rx} = \frac{E_p}{T_q}\frac{I_a^2 R}{4} \tag{68}$$

where R is the parallel resistance in Fig. 1(a). The noise density N can be written as the noise from R multiplied by some noise factor F which reflects the noise contribution from other sources (such as active devices) and depends on the actual topology of the SRA

$$N = \frac{4kTF}{R}. \tag{69}$$

Combining (57), (67)–(69), and (81) leads to the input signal power requirement for a given BER (or, equivalently, P_e)

$$P_{\min} = \frac{-16kTF\ln(2P_e)E_gE_p}{K_c^2T_q}. \quad (70)$$

This equation holds for general damping functions and pulse shapes. Using the definitions of E_g, E_p, and K_c, it can be used to determine the sensitivity of a receiver that uses a generic linear-mode, slope-controlled SRA. Solutions for two important cases discussed previously are given below, each using a ramp damping function.

1) Case 1, $p(t) = 1$, Ramp Damping: For this case, $K_c = \sigma_s\sqrt{2\pi}, E_g = \sigma_s\sqrt{2\pi}$, and $E_p = T_q$. Substituting these values in (70) yields

$$P_{\min} = -8kTF\ln(2P_e)\frac{\Omega_s}{\sqrt{\pi}}. \quad (71)$$

For a desired BER of 10^{-3}, (71) can be written in dBm as

$$P_{\min,\mathrm{dBm}} = -160\,\mathrm{dBm} + 10\log(F) + 10\log(\Omega_s). \quad (72)$$

As might be expected, (72) shows that the sensitivity degrades with higher SRA bandwidths as is common with other receiver types. This equation is independent of γ and is accurate as long as γ is *big enough*. In previous sections it was shown that reducing γ affects the frequency response by increasing the sidelobes. But, as shown in Fig. 7, even for values of γ as small as 2, the numerical frequency response matches the estimate up to 20 dB of attenuation, implying that the sensitivity functions presented are accurate for $\gamma \geq 2$.

The relationship between sensitivity and SRA bandwidth also affects the maximum data rate. The maximum data rate for an SRA receiver is $1/T_q$, and is achieved if the SRA is operated synchronously as in [5] and [11]. When synchronization is not used, the quench frequency must be greater than twice the bandwidth of the incoming signal since the SRA acts as a sampling device and must satisfy the Nyquist criterion. In either case, the bit rate is proportional to the quench frequency. For a particular value of γ (chosen to achieve a desired frequency response and gain), Ω_s is proportional to the quench frequency and there is a direct tradeoff between sensitivity and bit rate [11].

2) Case 2, $p(t) = g(t)$, Ramp Damping: If the optimal pulse shape is used, $K_c = T_q$ and $E_g = E_p = \sigma_s\sqrt{\pi}$, such that

$$P_{\min} = -16kTF\ln(2P_e)\frac{\pi\sigma_s^2}{T_q^3} \quad (73)$$

which can be written as

$$P_{\min} = -8kTF\ln(2P_e)\frac{\pi\Omega_s}{4\gamma^3}. \quad (74)$$

In dBm, this is equivalent to

$$P_{\min,\mathrm{dBm}} = -160\,\mathrm{dBm} + 10\log(F) + 10\log(\Omega_s) - 10\log\left(\frac{4\gamma^3}{\pi^{3/2}}\right). \quad (75)$$

In this case, the sensitivity is a very strong function of γ. To appreciate the tradeoff, recall from (46) that the incoming current is proportional to T_q/E_p. When Gaussian pulses are used, $T_q/E_p = 2\gamma/\sqrt{\pi}$. This means the peak-to-average ratio of the transmitted signal's amplitude (which is regulated for some standards) is proportional to γ. Some spread spectrum standards, however, allow for high peak-to-average ratios, making this technique very attractive. As mentioned already, the bit rate is proportional to the quench frequency and, therefore, inversely proportional to γ. However, for the case of a matched pulse, the relationship is favorable since reducing the bit rate by $2\times$ improves the sensitivity by $8\times$ (9 dB). Trading off sensitivity for bit rate by changing Ω_s is also an option, but it is important to note that for a pulsed signal the transmitted spectrum depends on Ω_s. When using Gaussian pulses, as in this analysis, the spectrum mask is set by $P(\omega - \omega_0)$, which would be Gaussian with a frequency standard deviation of Ω_s.

C. Using a Time Random Variable for Detection

The probability density functions described by (55) and (56) are defined for the amplitude of the SRA's envelope at the end of each quench cycle. In OOK receivers, the optimum threshold for determining whether the received bit is a *one* or a *zero* is the point at which the two PDFs intersect [13]. This point is approximately equal to $I_s/2$. To achieve the minimum BER, the demodulator in the receiver should be able to determine this value accurately. Doing so is most important when the input signal is small since this is when there is the greatest amount of overlap between the PDFs. When the input signal is large, the accuracy of the threshold is less critical since there is a wider range of values that will yield an acceptable BER.

The analysis up to now assumes that the SRA is a linear system and, as a result, I_s is linearly proportional to the input signal. However, if the SRA is actually highly nonlinear (typically compressive), I_s may not be a good measure of the input signal's amplitude, and choosing the optimal detection threshold becomes challenging. This is illustrated in Fig. 9. If the system is linear, the SRA's envelope is larger at time t_b when a *one* is received and smaller when a *zero* is received as in Fig. 9(d). If the system is highly compressive, however, the difference in amplitude at time t_b could be largely independent of the input signal's amplitude, making detection very difficult [as shown in Fig. 9(e)].

Ensuring linearity in the SRA can be achieved practically by using feedback to actively limit its gain to a sufficiently low value. Such techniques have been used for many decades [8], but present two main problems. First, the gain-control loop adds complexity and power consumption. Second, the system still requires that the SRA maintain a significant linear range. In modern systems, the primary benefit of SRAs is their ultralow-power operation, and a primary means of keeping the power consumption at a minimum is by reducing the supply voltage. The requirement to maintain a wide linear voltage range threatens these benefits since it typically requires a high supply voltage. This motivates a desire to achieve the benefits of SRAs mentioned up to now while eliminating the need for a wide linear voltage range.

One way of doing this is to use a different means of detection that extracts information from the input signal *before* the SRA's output envelope grows to the point of becoming nonlinear. This can be done by setting a voltage limit, V_T, inside the linear range of the SRA and measuring the length of time required for the SRA's envelope to grow to that level. This is

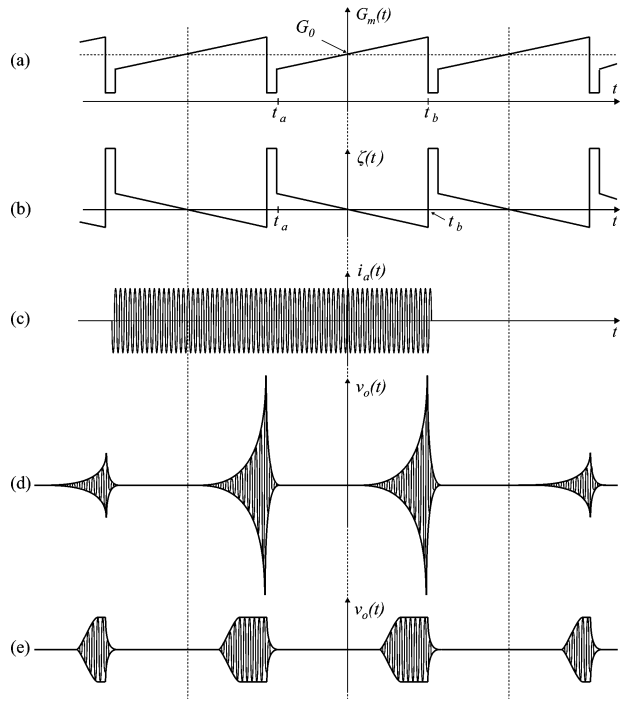

Fig. 9. SRA (a) transconductance $G_m(t)$, (b) damping function $\zeta(t)$, (c) input current $i_a(t)$, (d) output voltage for linear system $v_o(t)$, and (e) output voltage for compressive nonlinear system.

defined as the *trigger-time*, and it is a random variable [11]. For the case of a ramp damping function, setting $v_e(t) = V_T$ in (37) and solving for t yields the random variable

$$\mathbf{T_T} = \sqrt{2\sigma_s^2 \ln\left(\frac{I_0}{\mathbf{I_X}}\right)} \tag{76}$$

where

$$I_0 = \frac{V_T}{Z_0}. \tag{77}$$

As shown in Appendix B, the relationship between the probability density functions of $\mathbf{I_X}$ and $\mathbf{T_T}$ is

$$p_{\mathbf{T}}(t_T) = \left(I_0 \frac{t_T}{\sigma_s^2} e^{-\frac{t_T^2}{2\sigma_s^2}}\right) p_{\mathbf{I_X}}\left(I_0 e^{-\frac{t_T^2}{2\sigma_s^2}}\right). \tag{78}$$

Substituting (55) and (56) into (78) yields

$$p_{\mathbf{T}}(t_T \mid s_m = 0) = \left(\frac{I_0}{\sigma_X}\right)^2 \left(\frac{t_T}{\sigma_s^2}\right) e^{-\left(\frac{t_T^2}{\sigma_s^2} + \frac{I_0^2}{2\sigma_X^2} e^{\frac{-t_T^2}{\sigma_s^2}}\right)} \tag{79}$$

$$p_{\mathbf{T}}(t_T \mid s_m = 1) = \left(\frac{I_0}{\sigma_X\sqrt{2\pi}}\right) \left(\frac{t_T}{\sigma_s^2}\right) e^{-\left(\frac{t_T^2}{2\sigma_s^2} + \frac{1}{2\sigma_X^2}(I_0 e^{\frac{-t_T^2}{2\sigma_s^2}} - I_s)^2\right)}. \tag{80}$$

While the density functions of $\mathbf{T_T}$ are far messier than those of $\mathbf{I_X}$, they allow accurate detection even when the SRA is highly nonlinear. This is because V_T can be set to a small value such that the trigger-time is extracted before the SRA's amplitude causes nonlinearities in the system. Furthermore, the probability of error in detection must, intuitively, be the same as if $\mathbf{I_X}$ were used since there is a one-to-one mapping between their densities.

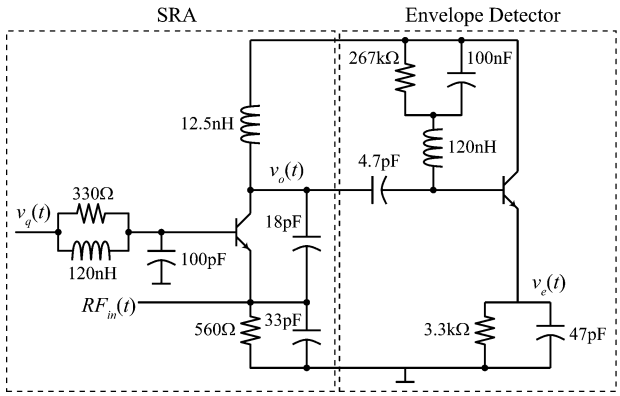

Fig. 10. Schematic of SRA and envelope detector.

V. Measurement Results

Fig. 10 shows the schematic for a simple SRA based on a common-base Colpitts oscillator and an envelope detector. The resonant frequency was arbitrarily chosen in the 400-MHz frequency range reserved for Medical Implant Communication Services (402–405 MHz), but much higher frequencies could be used. Typically an LNA is used to isolate the antenna from the SRA so that its output signal is not radiated. But to better characterize the SRA and verify the theory presented, the LNA was excluded. A common-base configuration was chosen for the SRA to facilitate input matching, and the quench signal used to control the damping function was connected to the base through a simple low-pass filter. A high Q inductor was used in the resonant tank so that the effective parallel resistance is dominated by well controlled resistances (i.e., r_e of the transistor, 50 Ω source impedance, and 560 Ω bias resistor). While this is suboptimal for performance, it allows for more accurate performance prediction. The envelope detector is similar to [5] and a sawtooth damping function similar to Fig. 9(b) was generated using an arbitrary waveform generator. A low supply voltage of 1.0 V was used to show that accurate detection is possible using the trigger-time technique despite a very narrow linear range.

Fig. 11 shows the output of the envelope detector for different input power levels of CW signals at the resonant frequency of the SRA. The dashed lines show the predicted shape of the envelope compared to the measurement results shown by the solid lines. Two sample signals are shown for the case when no input signal was used to show the random nature of the signal amplitude. Note that the measured results are in agreement with predictions when the SRA envelope is small, but diverge significantly as the nonlinearities of the system lead to signal compression. If this SRA had been designed to function strictly in the linear region, the SRA gain would have been set much lower (by reducing γ or Ω_s, for example) or the supply voltage would have been made larger. Using the trigger-time technique eliminated the need to do so. Instead, the threshold voltage was set to a low value ($V_T = 15$ mV) and the trigger-time was measured using the histogram function of a digital oscilloscope. From Fig. 11 it

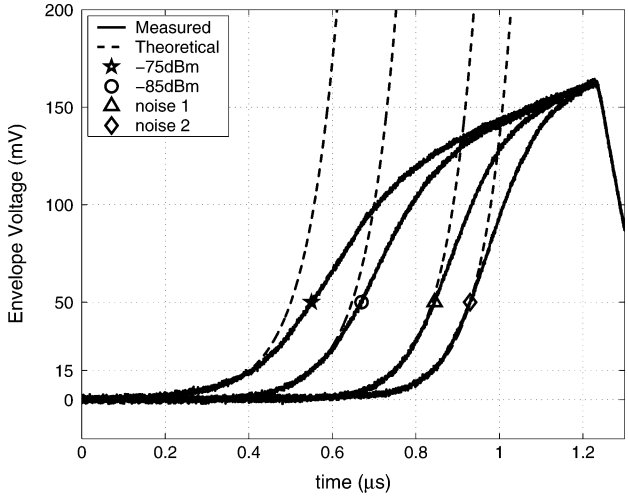

Fig. 11. Theoretical and measured envelope detector waveforms for -75 dBm and -85 dBm CW input signals and two sample waveforms for no input signal (i.e., only noise).

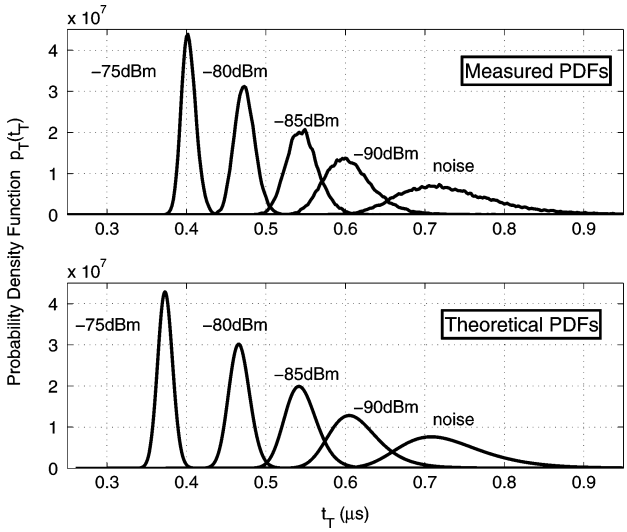

Fig. 12. Measured and theoretical probability density functions for the random variable t_T.

is clear that there is good agreement between theory and measured results for values of $v_e(t)$ below 15 mV, so the measured trigger-time PDFs should be in agreement with theory.

Fig. 12 shows the measured and theoretical probability density functions of $\mathbf{T_T}$ for varying input signal levels. For this measurement, the quench signal of the SRA was set to 300 kHz, and its slope resulted in a value of $4.4\ \text{MHz}\sqrt{\text{rad}}$ for Ω_s. The density functions were extracted by weighting the time histograms such that they integrate to unity. The theoretical distribution functions of $\mathbf{T_T}$ are also plotted according to (79) and (80). Clearly, there is excellent agreement between the theoretical and measured signals for input power levels up to -80 dBm. For larger input signals the theory becomes less accurate because t_T is no longer sufficiently larger than σ_s, as required for the convolution approximation to be accurate. This is not important, however, since selecting the detection threshold is trivial when the input signal is large (i.e., there is a wide range of values for which the BER will meet requirements). In contrast, accurately modeling the PDFs for low input signal levels is very important since it enables the selection of the optimum detection threshold, resulting in the best sensitivity. Fig. 12 shows there is excellent agreement between theory and measurements for small input signal levels. Furthermore, the -80 dBm value is only specific to this design and only important in the sense that it represents an input signal significantly larger than the sensitivity level. For receiver designs with much lower or higher sensitivities, the theoretical PDFs are expected to match for a wide enough range of input signal values to allow for optimal threshold determination and, thereby, optimal sensitivity.

The BER, which is equivalent to the probability of error P_e, was calculated by finding the optimal threshold for a given input power and integrating the portion of each PDF that was on the *wrong side*. For example, for a -90-dBm input signal, the optimum threshold was determined to be 0.66 μs. The probability of error was found by integrating the -90 dBm PDF from $t = 0.66\ \mu$s to $t = 1\ \mu$s and adding the result to the integral of the noise PDF from 0 to 0.66 μs. Using this technique, it was determined that a BER of 10^{-3} was achieved for a -87-dBm CW input signal. This corresponds to an OOK modulated input signal level of -90 dBm (since its average power would be 3 dB lower), which matches the predicted value given by (72) for a noise factor of $F = 2.3$ (3.6 dB).

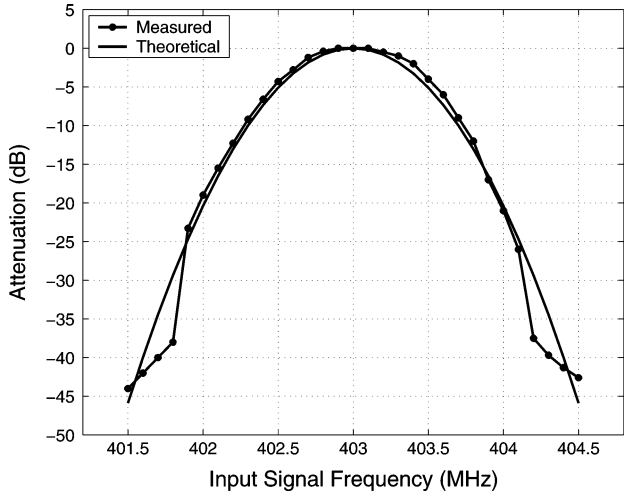

Fig. 13. Frequency response of the SRA for $\Omega_s/(2\pi) = 480\ \text{kHz}/\sqrt{\text{rad}}$.

The dc current consumption of the SRA was 500 μA for a total power consumption of 500 μW. The theoretical noise factor was calculated using techniques similar to those used in [11]. The effective resistance at the emitter of the SRA transistor is the parallel combination $R_e = R_s \| r_e \| 560\,\Omega = 24.4\,\Omega$, where $R_s = 50\ \Omega$ is the source impedance of the signal generator and $r_e = 25.9\ \text{mV}/500\ \mu\ \text{A} = 52\ \Omega$ is the small signal emitter resistance of the BJT. The effective resistance across the resonator is $R_{\text{eff}} = R_e((18\ \text{pF} + 33\ \text{pF})/18\ \text{pF})^2 = 196\,\Omega$ [14]. The BJT's thermal noise density is given by $N_{\text{bjt}} = 2qI_D = 160 \times 10^{-24}$ and the resistor's noise density is given by $N_{\text{res}} = 4kT/R_{\text{eff}} = 84.5 \times 10^{-24}$. The noise factor is, therefore, $F = N_{\text{tot}}/N_{\text{res}} = 2.9$ (4.6 dB). This means that the theoretical noise factor and the measured noise factor are within 1 dB, confirming the accuracy of the theory.

Fig. 13 shows the filtering characteristics of the SRA resulting from the attenuating effect of frequency mismatch between the

SRA's resonator and the input signal. For this measurement, the quench signal of the SRA was set to 300 kHz, and its slope resulted in a value of $2\pi \times 480\,\text{kHz}\sqrt{\text{rad}}$ for Ω_s. This, in effect, describes the selectivity of the SRA. The measurement was made by finding the average value of t_T for a -80-dBm CW input signal at 403 MHz (the SRA's resonant frequency) and then sweeping the frequency and power level of the input signal. For each frequency, the input signal power was swept until the value of t_T was the same as for the reference signal (-80 dBm, 403 MHz). Measured results show excellent matching compared to (43) up to about 25 dB of attenuation. Beyond such levels, other phenomena, including the effects of finite γ, begin to dominate, making the measurement less accurate.

VI. Conclusion

A frequency-domain approach to analyzing super-regenerative amplifiers has been presented. Sensible approximations have been made that enable a convolution model to describe part of the time-varying solution. The convolution model was used to find the SRA's response to arbitrary deterministic and stochastic signals, with specific examples of its response to a single sinusoid, multiple sinusoids, a pulsed sinusoid, and AWGN. These solutions were then used to find the sensitivity of a synchronous SRA receiver to an OOK signal with and without pulse shaping, and the benefits of both cases were discussed. The probability density functions were found for a trigger-time random variable that can be used for OOK detection and helps avoid the problems associated with SRA nonlinearity. Finally, experimental data was presented that matched the theory with excellent agreement.

Appendix A
Convolution Yielding the Variance of $\mathbf{I_X}$

The first step to finding the variance of $\mathbf{I_X}$ is to solve the convolution

$$\begin{aligned}\overline{|X(\omega)|^2} &= \frac{N\omega^2}{4\pi} * |G(\omega)|^2 \\ &= \frac{N}{4\pi}\int_{-\infty}^{\infty}(\omega-\lambda)^2|G(\lambda)|^2 d\lambda. \end{aligned} \tag{81}$$

Expanding this solution and substituting $\omega = \omega_0$ yields

$$\begin{aligned}\overline{|X(\omega_0)|^2} = \frac{N}{4\pi}\Bigg(&\int_{-\infty}^{\infty}\omega_0^2|G(\lambda)|^2 d\lambda \\ &- \int_{-\infty}^{\infty}2\omega_0\lambda|G(\lambda)|^2 d\lambda + \int_{-\infty}^{\infty}\lambda^2|G(\lambda)|^2 d\lambda\Bigg). \end{aligned} \tag{82}$$

Since $|G(\omega)|$ is an even function, the second integral can be discarded. A further simplification can be made by observing that $|G(\omega)|$ is a baseband signal, and therefore $|G(\lambda)|$ becomes very small for values of λ well below ω_0. As a result, over the range of λ for which $|G(\lambda)|$ has a significant value, the λ^2 term in the third integral is much smaller than the ω_0^2 term in the first integral. This means the third integral can also be discarded resulting in the simplified solution for the variance σ_X^2

$$\sigma_X^2 = \overline{|X(\omega_0)|^2} = \frac{1}{2}N\omega_0^2 E_g \tag{83}$$

where E_g is the energy of the sensitivity function defined as

$$E_g = \frac{1}{2\pi}\int_{-\infty}^{\infty}|G(\omega)|^2 d\omega = \int_{-\infty}^{\infty} g^2(t)dt. \tag{84}$$

Appendix B
Solving for the PDF of $\mathbf{T_T}$

In Section IV-C the trigger-time random variable, $\mathbf{T_T}$ was introduced to help alleviate some of the problems created by the nonlinearity of the SRA's active elements. $\mathbf{T_T}$ is related to $\mathbf{I_X}$ through (76), and its probability density function is the derivative of its cumulative distribution function [15] given by

$$F_{\mathbf{T}}(t_T) = P\{\mathbf{T_T} \le t_T\} \tag{85}$$

$$= P\left\{\sqrt{2\sigma_s^2 \ln(I_0/\mathbf{I_X})} \le t_T\right\} \tag{86}$$

$$= P\left\{\mathbf{I_X} \ge I_0 e^{-\frac{t_T^2}{2\sigma_s^2}}\right\} \tag{87}$$

$$= 1 - F_{\mathbf{X}}\left(I_0 e^{-\frac{t_T^2}{2\sigma_s^2}}\right). \tag{88}$$

Differentiating (88) with respect to t_T yields the PDF of $\mathbf{T_T}$ with respect to the PDF of $\mathbf{I_X}$

$$p_{\mathbf{T}}(t_T) = \left(I_0 \frac{t_T}{\sigma_s^2} e^{-\frac{t_T^2}{2\sigma_s^2}}\right) p_{\mathbf{I_X}}\left(I_0 e^{-\frac{t_T^2}{2\sigma_s^2}}\right). \tag{89}$$

Acknowledgment

The authors would like to thank William Sanchez, Patrick Mercier, and Manish Bhardwaj for valuable discussions and comments.

References

[1] E. H. Armstrong, "Some recent developments of regenerative circuits," in *Proc. IRE*, Aug. 1922, vol. 10, pp. 244–260.

[2] J. Y. Chen, M. P. Flynn, and J. P. Hayes, "A fully integrated auto-calibrated super-regenerative receiver in 0.13-μm CMOS," *IEEE J. Solid-State Circuits*, vol. 42, no. 9, pp. 1976–1985, Sep. 2007.

[3] P. Favre, N. Joehl, A. Vouilloz, P. Deval, C. Dehollain, and M. J. Declercq, "A 2-V 600-μA 1-GHz BiCMOS super-regenerative receiver for ISM applications," *IEEE J. Solid-State Circuits*, vol. 33, no. 12, pp. 2186–2196, Dec. 1998.

[4] F. X. Moncunill-Geniz, P. Palá-Schönwälder, and O. Mas-Casals, "A generic approach to the theory of superregenerative reception," *IEEE Trans. Circuits Syst. I*, vol. 52, no. 1, pp. 54–70, Jan. 2005.

[5] F. X. Moncunill-Geniz, P. Palá-Schönwälder, C. Dehollain, N. Joehl, and M. Declercq, "An 11-Mb/s 2.1 mW synchronous superregenerative receiver at 2.4 GHz," *IEEE Trans. Microw. Theory Tech.*, vol. 55, no. 6, pp. 1355–1362, Jun. 2007.

[6] B. Otis, Y. H. Chee, and J. Rabaey, "A 400 μW-RX, 1.6 mW-TX super-regenerative transceiver for wireless sensor networks," in *IEEE Int. Solid-State Circuits Conf. (ISSCC) Dig. Tech. Papers*, San Francisco, CA, Feb. 2005, pp. 396–397 and 606.

[7] A. Vouilloz, M. Declercq, and C. Dehollain, "A low-power CMOS super-regenerative receiver at 1 GHz," *IEEE J. Solid-State Circuits*, vol. 36, no. 3, pp. 440–451, Mar. 2001.

[8] J. R. Whitehead, *Super-Regenerative Receivers*, 1st ed. Cambridge, U.K.: Cambridge Univ. Press, 1950.

[9] F. X. Moncunill-Geniz and P. Palá-Schönwälder, "Performance of a DSSS superregenerative receiver in the presesnce of noise and interference," in *IEEE Int. Symp. on Circuits and Systems (ISCAS) Proc.*, Island of Kos, Greece, May 2006, pp. 5684–5687.

[10] D. M. Pelissier and M. J. Soen, "A new pulse detector based on super-regeneration for UWB low power applications," in *Proc. IEEE Int, Conf. Ultra-Wideband*, Waltham, MA, Sep. 2006, pp. 639–644.
[11] J. L. Bohorquez, J. L. Dawson, and A. P. Chandrakasan, "A 350 μW CMOS MSK transmitter and 400 μW OOK super-regenerative receiver for medical implant communications," *IEEE J. Solid-State Circuits*, vol. 44, no. 4, pp. 1248–1259, Apr. 2009.
[12] U. L. Rohde and A. K. Poddar, "Super-regenerative receiver," in *IEEE Conf. Electron Devices and Solid-State Circuits, EDSSC 2007*, Tainan, Taiwan, Dec. 2007, pp. 263–266.
[13] B. P. Lathi, *Modern Digital and Analog Communication Systems*, 3rd ed. New York, NY: Oxford Univ. Press, 1998, pp. 116–129, 463, 595–597.
[14] T. H. Lee, *The Design of CMOS Radio-Frequency Integrated Circuits*, 2nd ed. Cambridge, U.K.: Cambridge Univ. Press, 2004, pp. 610–620.
[15] A. Leon-Garcia, *Random Processes for Electrical Engineers*, 2nd ed. Reading, MA: Addison-Wesley, 1993, pp. 119–126.

Jose L. Bohorquez (S'04) received the B.S. and M.S. degrees in electrical engineering from the University of Florida, Gainesville, in 2002 and 2004. In 2006, he began doctoral studies at the Massachusetts Institute of Technology (MIT), Cambridge, where his research has focused on ultralow-power systems for medical implants.

He has held internships at APA Wireless, Lockheed Martin, and GE Healthcare, and in 2004 joined BitWave Semiconductor where he designed analog and radio-frequency blocks for a reconfigurable transceiver.

Mr. Bohorquez has received several awards including the International Engineering Consortium's William L. Everitt Student Award of Excellence, the Semiconductor Research Corporation/IBM Fellowship, and the MIT Presidential Fellowship.

Anantha P. Chandrakasan (M'95–SM'01–F'04) received the B.S., M.S., and Ph.D. degrees in electrical engineering and computer sciences from the University of California, Berkeley, in 1989, 1990, and 1994, respectively.

Since September 1994, he has been with the Massachusetts Institute of Technology, Cambridge, where he is currently the Joseph F. and Nancy P. Keithley Professor of Electrical Engineering. He is a coauthor of *Low Power Digital CMOS Design* (Kluwer Academic, 1995) and *Digital Integrated Circuits* (Pearson Prentice-Hall, 2003, 2nd ed.). He is also a coeditor of *Low Power CMOS Design* (IEEE Press, 1998), *Design of High-Performance Microprocessor Circuits* (IEEE Press, 2000), *Leakage in Nanometer CMOS Technologies* (Springer, 2005), and *Sub-threshold Design for Ultra-Low Power Systems* (Springer, 2006). His research interests include low-power digital integrated circuit design, wireless microsensors, ultrawideband radios, and emerging technologies.

Dr. Chandrakasan has received several awards including the 1993 IEEE Communications Society's Best Tutorial Paper Award, the IEEE Electron Devices Society's 1997 Paul Rappaport Award for the Best Paper in an EDS publication during 1997, the 1999 Design Automation Conference Design Contest Award, and the 2004 DAC/ISSCC Student Design Contest Award. He has served as a Technical Program Co-Chair for the 1997 ISLPED, VLSI Design'98, and the 1998 IEEE Workshop on Signal Processing Systems. He was the Signal Processing Subcommittee Chair for ISSCC 1999–2001, the Program Vice-Chair in 2002, the Program Chair in 2003, the Technology Directions Subcommittee Chair in 2004–2007, and the Technology Directions Chair in 2008. He was an Associate Editor for the IEEE J. SOLID-STATE CIRCUITS from 1998 to 2001, and serves on the SSCS Administrative Committee as the Meetings Committee Chair.

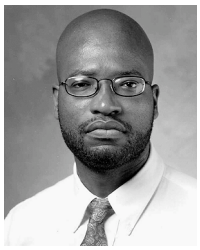

Joel L. Dawson (M'97) received the S.B. degree in electrical engineeringt from the Massachusetts Institute of Technology (MIT), Cambridge in 1996, and the M.Eng. degree from MIT in electrical engineering and computer science in 1997. He went on to pursue further graduate studies at Stanford University, Stanford, CA, where he received the Ph.D. degree in electrical engineering for his work on power amplifier linearization techniques.

He is currently an Associate Professor in the Department of Electrical Engineering and Computer Science at MIT. Before joining the faculty at MIT in 2004, he spent one year at Aspendos Communications, a startup company that he cofounded. He continues to be active in the industry as both a technical and legal consultant.

Prof. Dawson received the NSF CAREER Award in 2008.